

# Theoretical study of ArH<sup>+</sup> dissociative recombination and electron-impact vibrational excitation

A. Abdoulanziz,<sup>1</sup> F. Colboc,<sup>1</sup> D. A. Little,<sup>2</sup> Y. Moulane,<sup>3,4</sup> J. Zs. Mezei,<sup>1,5,6</sup> E. Roueff,<sup>7</sup> J. Tennyson,<sup>2</sup> I. F. Schneider<sup>1,8</sup> and V. Laporta<sup>1,2</sup>★

<sup>1</sup>Laboratoire Ondes et Milieux Complexes, CNRS–Université du Havre–Normandie Université, 76058 Le Havre, France

<sup>2</sup>Department of Physics and Astronomy, University College London, London WC1E 6BT, UK

<sup>3</sup>Oukaimden Observatory, High Energy Physics and Astrophysics Laboratory, Cadi Ayyad University, Marrakech, Morocco

<sup>4</sup>Space sciences, Technologies & Astrophysics Research Institute, University of Liège, Liège, Belgium

<sup>5</sup>Laboratoire des Sciences des Procédés et des Matériaux, CNRS–Université Paris 13–USPC, 93430 Villetaneuse, France

<sup>6</sup>Institute of Nuclear Research, Hungarian Academy of Sciences, Debrecen, Hungary

<sup>7</sup>Sorbonne Université, Observatoire de Paris, Université PSL, CNRS, LERMA, F-92190, Meudon, France

<sup>8</sup>Laboratoire Aimé-Cotton, CNRS–Université Paris-Sud–ENS Cachan–Université Paris-Saclay, 91405 Orsay, France

Accepted XXX. Received YYY; in original form ZZZ

## ABSTRACT

Cross sections are presented for dissociative recombination and electron-impact vibrational excitation of the ArH<sup>+</sup> molecular ion at electron energies appropriate for the interstellar environment. The R-matrix method is employed to determine the molecular structure data, *i.e.* the position and width of the resonance states. The cross sections and the corresponding Maxwellian rate coefficients are computed using a method based on the Multichannel Quantum Defect Theory. The main result of the paper is the very low dissociative recombination rate found at temperatures below 1000K. This is in agreement with the previous upper limit measurement in merged beams and offers a realistic explanation to the presence of ArH<sup>+</sup> in exotic interstellar conditions.

**Key words:** ArH<sup>+</sup> – dissociative recombination – vibrational excitation – interstellar medium

## 1 INTRODUCTION

The presence of the ArH<sup>+</sup> molecular cation, argonium, in interstellar medium (ISM) was reported for the first time by Barlow *et al.* (2013), who detected <sup>36</sup>ArH<sup>+</sup> 617.525 GHz ( $J = 1 - 0$ ) and 1234.603 GHz ( $J = 2 - 1$ ) emission lines in spectra from the Crab Nebula using the data from Herschel mission. That supernova remnant is known to contain both molecular hydrogen and regions of enhanced ionized argon emission. After this first noble gas molecular ion detection, Schilke *et al.* (2014) realized that the still unidentified absorption transition at 617.5 GHz observed in diffuse gas toward several sources such as Sg B2, and various PRISMA sources (W31C, W49N, W51e, ...), was in fact due to argonium with <sup>36</sup>Ar. Moreover, features of <sup>38</sup>ArH<sup>+</sup> were subsequently found in Sg B2(M) as well and, consequently, Schilke *et al.* suggested that argonium is ubiquitous in the ISM. More recently, Müller *et al.* (2015) made extragalactic detections of the <sup>36</sup>Ar and <sup>38</sup>Ar isotopologues of argonium through absorption studies of a foreground galaxy

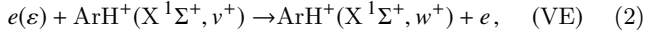
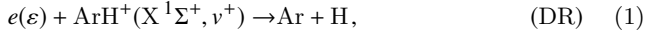
at  $z = 0.89$  along two different lines of sight toward PKS 1830-211 within the band 7 of the ALMA interferometer, including the corresponding redshifted transitions.

The possible formation/destruction processes linked to ArH<sup>+</sup> are discussed by Neufeld & Wolfire (2016) who emphasized that ArH<sup>+</sup> is a good tracer of the almost purely atomic diffuse ISM in the Milky Way. However, an important missing piece of information remains the unknown value of the dissociative recombination rate coefficient of that molecular ion. An upper limit of  $10^{-9}$  cm<sup>3</sup> s<sup>-1</sup> for electron collision energies below about 2 eV was reported by Mitchell *et al.* (2005) who performed a storage ring measurement. Mitchell *et al.* also gave the corresponding theoretical potential curves. That upper limit value is adopted in the presently available astrochemical models for galactic diffuse clouds (Neufeld & Wolfire 2016) whereas Priestley *et al.* (2017) introduce a lower value ( $10^{-11}$  cm<sup>3</sup> s<sup>-1</sup>) to interpret the Crab nebula observations. Photodissociation of ArH<sup>+</sup>, another potential destruction mechanism, was studied theoretically by Alekseyev *et al.* (2007) and the corresponding photodissociation rate was shown to be moderate, *i.e.*  $9.9 \cdot 10^{-12}$  s<sup>-1</sup> in the unshielded mean ultraviolet interstellar ra-

★ E-mail: vincenzo.laporta@univ-lehavre.fr (VL)

diation field (Roueff et al. 2014). In addition to these, the rotational excitation due to electron impact has been studied by Hamilton et al. (2016).

In this paper, we investigate theoretically the dissociative recombination (DR) process of  $\text{ArH}^+$  through *ab initio* methods, including the dependence on the vibrational excitation of the target molecular ion and, in the same energy range, the competitive process of vibrational excitation (VE) by electron impact, *i.e.*:



where  $\varepsilon$  is the incident electron energy,  $v^+$  and  $w^+$  represent the initial and final vibrational quantum numbers respectively corresponding to the ground electronic state  $X^1\Sigma^+$  of  $\text{ArH}^+$ .

The manuscript is organized as follows: in Section 2 the theoretical model used to characterize the  $\text{ArH}^{**}$  resonant states is presented and in Section 3 the results concerning the cross sections and the corresponding rate coefficients are discussed. Finally the conclusions, in Section 4, close the paper.

## 2 THEORETICAL MODEL

A theoretical study of the  $\text{ArH}^+$  electronic excited states was performed by Stolyarov & Child (2005); Jungen et al. (1997), and more recently Kirrander et al. (2006), explored  $\text{ArH}$  Rydberg states.

In the present work, *ab initio*  $\text{ArH}^+$  calculations were performed using MOLPRO and an aug-cc-pVQZ (AVQZ) Gaussian type orbital (GTO) basis set at the complete active space (CAS) self-consistent field (SCF) level of theory. These calculations provided input orbitals for the electron-ion scattering calculations. All calculations were performed in  $C_{2v}$  symmetry, which is the highest allowed by MOLPRO and the polyatomic R-matrix code for an asymmetric linear molecule.

The potential energy curves and the widths for the  $\text{ArH}^{**}$  resonant states were calculated using the R-matrix method (Tennyson 2010) as implemented in UKRMol code (Carr et al. 2012). The general approach follows closely the treatment of  $\text{N}_2^{**}$  by Little & Tennyson (2014) which provided the input for  $\text{N}_2^+$  DR calculations (Little et al. 2014). The  $\text{ArH}^+$  target states were represented using the AVQZ GTO basis set and a CAS in which the Ar  $1s^2 2s^2 2p^6$  electrons were frozen and the remaining 8 electrons were distributed as  $(4\sigma, 5\sigma, 6\sigma, 2\pi)^8$ . The  $3\pi$  virtual orbital was retained to augment the continuum orbitals in the scattering calculation.

The scattering calculations used an R-matrix sphere of radius  $10 a_0$ . Continuum basis functions were represented using GTOs placed at the center of this sphere and contained up to  $g$  orbitals ( $\ell \leq 4$ ) (Faure et al. 2002). Close-coupling calculations built on the target CAS (Tennyson 1996) and an expansion of the 8 lowest states of each ( $C_{2v}$ ) symmetry were retained for the outer region calculations. In this latter region, calculations were repeated for the internuclear separations  $2.2 < R < 15 a_0$  and for symmetries corresponding to  $^2\Sigma^+$ ,  $^2\Pi$  and  $^2\Delta$  scattering channels.

The outer region calculations explicitly considered the

$\mu$ (a.u.)	1791.94		
$R_{eq}$ ( $a_0$ )	2.419 (2.419)		
$D_e$ (eV)	4.039 (4.025)		
$D_0$ (eV)	3.8725		
$v^+$	$\epsilon_{v^+}$ (eV)	$v^+$	$\epsilon_{v^+}$ (eV)
0	0.000	12	2.949
1	0.321	13	3.110
2	0.627	14	3.258
3	0.919	15	3.393
4	1.197	16	3.513
5	1.461	17	3.617
6	1.712	18	3.703
7	1.949	19	3.770
8	2.174	20	3.817
9	2.387	21	3.846
10	2.587	22	3.861
11	2.774		

**Table 1.** Molecular constants (reduced mass, equilibrium distance and dissociating energies) for  $^{40}\text{ArH}^+$  in its ground electronic state and the energies of the corresponding vibrational levels. The comparison with the experimental data of Hotop et al. (1998) given in brackets is reported.

20 lowest target states. R-matrices were propagated to  $100.1 a_0$  and then fitted to an asymptotic form. Resonance positions and widths were determined by automated fitting of the eigenphase sums to a Breit-Wigner form using program RESON (Tennyson & Noble 1984). Couplings were determined from the resonance widths  $\Gamma$  using the formula:

$$V(R) = \sqrt{\frac{\Gamma(R)}{2\pi}}. \quad (3)$$

Figure 1 shows the R-matrix results for resonance positions (upper panel), couplings (middle panel) and quantum defect (lower panel). The corresponding molecular data are given in Table 1. These data form the input for the Multi-channel Quantum Defect Theory (MQDT) step of the calculations. Linear extrapolation was adopted for the couplings in order to extend the internuclear distances range below  $2.2 a_0$  to  $1.6 a_0$ .

$\text{ArH}^+$  is a closed shell system so no spin-orbit (SO) splitting effects are expected in its ro-vibrational levels. Conversely, SO effects may be important in the non- $\Sigma$  resonances and are well characterized for the Ar asymptotic states. In particular, the  $\text{Ar}(^2P_{3/2}^0, 4s)$  and  $\text{Ar}(^2P_{1/2}^0, 4s)$  show SO splittings of 0.075 eV and 0.105 eV, respectively (Kramida et al. 2018). Our calculations are non-relativistic and therefore neglect SO effects; we assume the calculated R-matrix resonances converge on the lowest component of the Ar doublets at large internuclear distances. Table 2 shows the asymptotic limits of the  $\text{ArH}^{**}$  resonant states considered below.

The MQDT method (Giusti 1980; Guberman & Giusti-Suzor 1991; Chakrabarti et al. 2013; Motapon et al. 2014; Little et al. 2014; Epée Epée et al. 2015) was used to study the processes (1) and (2). Within this approach, the corresponding cross sections are expressed in terms of S-matrix

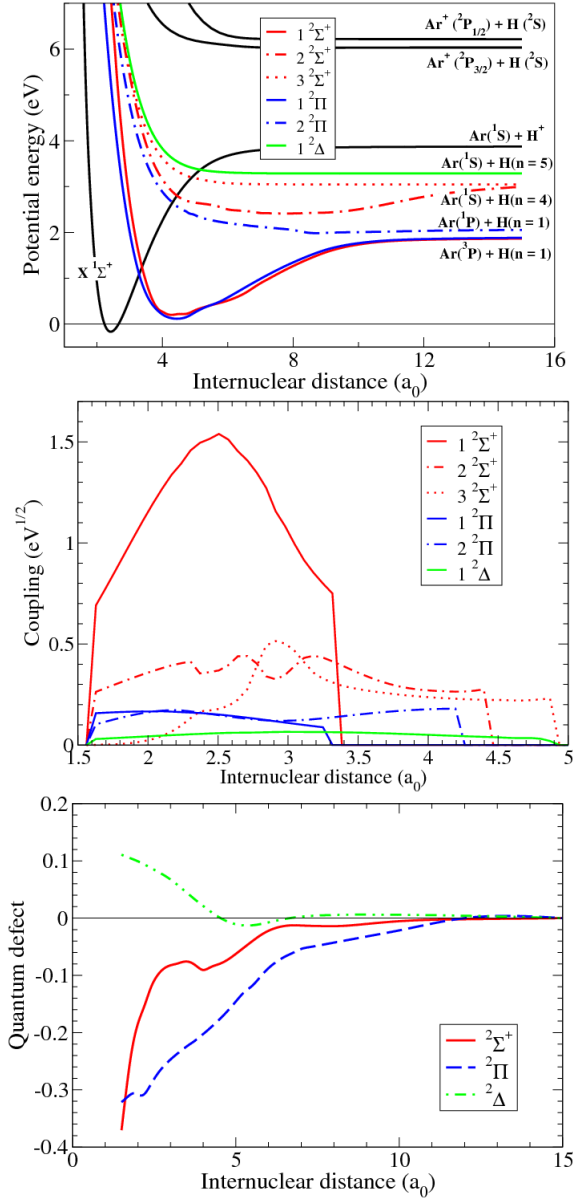


**Figure 1.** Potential energy curves, couplings and quantum defects used in the present calculations. The ArH<sup>+</sup> potential curves - ground state, X<sup>1</sup>Σ<sup>+</sup>, and the lowest excited electronic states - are displayed as black lines. The molecular data sets for the different symmetries of the neutral system are displayed with different colors: 2Σ in red, 2Π in blue and 2Δ in green.

Channel	Energy (eV)	Symmetries
Ar <sup>(3)P</sup> + H(n = 1)	-2.00 (-2.05)	1 <sup>2</sup> Σ <sup>+</sup> , 1 <sup>2</sup> Π
Ar <sup>(1)P</sup> + H(n = 1)	-1.81 (-1.87)	2 <sup>2</sup> Π
Ar <sup>(1)S</sup> + H(n = 4)	-0.87 (-0.85)	2 <sup>2</sup> Σ <sup>+</sup> , 3 <sup>2</sup> Σ <sup>+</sup>
Ar <sup>(1)S</sup> + H(n = 5)	-0.58 (-0.54)	1 <sup>2</sup> Δ

**Table 2.** Asymptotic limits of the ArH<sup>\*\*</sup> resonant states relevant for the low-energy impact collisions. The energy is expressed with respect to the asymptotic limit of the ground electronic state of ArH<sup>+</sup>. The experimental energy values from the NIST database (Kramida et al. 2018) are given in brackets for comparison.

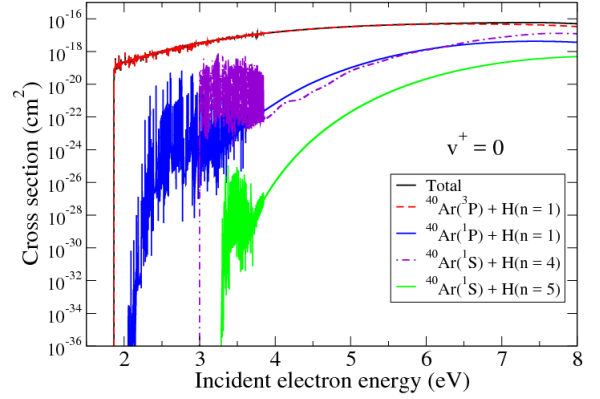


**Figure 2.** Dissociative recombination of vibrationally relaxed ArH<sup>+</sup>. Broken colored lines: The contributions coming from all the dissociative states having the same asymptotic atomic limit. Solid black line (partially hidden by the red curve): Total cross section coming from the sum over all the available dissociative states.

elements as:

$$\sigma_{v^+}(\varepsilon) = \frac{\pi}{4\varepsilon} \sum_{sym, \Lambda, l, j} \rho^{sym, \Lambda} \left| S_{d_j, l v^+}^{sym, \Lambda} \right|^2, \quad (4)$$

$$\sigma_{v^+, w^+}(\varepsilon) = \frac{\pi}{4\varepsilon} \sum_{sym, \Lambda, l, l'} \rho^{sym, \Lambda} \left| S_{l' w^+, l v^+}^{sym, \Lambda} - \delta_{l, l'} \delta_{v^+, w^+} \right|^2, \quad (5)$$

where the summation is extended over all symmetries (*sym*: spin, inversion for homonuclear molecules) of the neutral system, projection of the total electronic angular momentum on the internuclear axis  $\Lambda$ , and partial waves  $l/l'$  of the incident/scattered electron, and  $\rho^{sym, \Lambda}$  is the ratio between the multiplicities of the neutral system and of the target ion.

The most abundant isotope of argon in the Earth's atmosphere is <sup>40</sup>Ar whereas in the ISM <sup>36</sup>Ar and <sup>38</sup>Ar isotopes are preponderant. In the present work, we deal with vibrational processes and, due to the small relative variation of the reduced mass from one isotopologue to another - as a consequence of the huge atomic mass of the Ar isotopes - we expect these effects to be negligible. In order to verify this, we performed calculations for different isotopologues of ArH<sup>+</sup> and the relative difference between the rate coefficients was found to be below 1%.

### 3 RESULTS AND DISCUSSION

Figure 2 displays the DR cross sections for ArH<sup>+</sup> v<sup>+</sup> = 0, namely the total one and the partial contributions corresponding to the asymptotic channels of resonant states. It can be noted that the main contribution arises from the Ar<sup>(3)P</sup> + H(n = 1) channel. One reason for this is that, as shown in Table 2, this exit channel gathers contributions coming from two states - 1<sup>2</sup>Σ<sup>+</sup> and 1<sup>2</sup>Π - instead of one state, as is the case of the exit channels Ar<sup>(1)P</sup> + H(n = 1) and Ar<sup>(1)S</sup> + H(n = 5). One can argue that - as shown in Table 2 - the channel Ar<sup>(1)S</sup> + H(n = 4) is the asymptotic limit of two states, as the Ar<sup>(3)P</sup> + H(n = 1) one. However, the coupling of the 1<sup>2</sup>Σ<sup>+</sup> state with the electron/ion continuum (see Fig. 1) is about three times larger than the other ones.

Figures 3(a) and (b) display, respectively, the results for DR cross sections and the corresponding rate coefficients for  $\nu^+ = 0, 1, 2$ . Two features can be noted:

(i) The resonant structures present in the cross sections correspond to the temporary captures into singly-excited Rydberg states  $\text{ArH}^*$ , and they cease to appear when the electron energy reaches the dissociation energy of  $\text{ArH}^+$  ( $\nu^+ = 0, 1, 2$ );

(ii) For a vibrationally relaxed target, the dissociation channels are closed for energies of the incident electron below 1.8 eV. For the ion situated on one of the next 8 excited vibrational states, the threshold decreases progressively, and the DR becomes exothermic for vibrational levels equal or higher to 9 only. This particular energetic situation explains the particular behavior of the computed rate coefficients displayed in Fig. 3(b), namely the very low values and the "explosive" increase below 2000 K.

In order to validate the results, Fig. 4 shows the anisotropic DR rate coefficient for  $\nu^+ = 0$ , calculated by considering the electron beam with a longitudinal temperature  $kT_{\parallel} \approx 0.5$  eV and a transverse temperature  $kT_{\perp} \approx 25$  meV, compared to the experimental data from the storage ring by Mitchell et al. (2005). We note that the agreement is quite satisfactory at energies greater than  $\sim 3$  eV within the 20% experimental error. At lower energies our calculated rates are smaller than the experimental ones: This can derive from bad detected signal as stated by the authors.

Figure 5 displays the DR cross section compared to the competitive process of VE for one quantum excitation in the same energy range. The main feature is that, at energies just above the opening of the dissociative channels, the VE cross section is larger than the corresponding DR starting from the same vibrational level.

We also checked the isotopic effect by replacing  $\text{ArH}^+$  by  $\text{ArD}^+$ , which results in a variation of the reduced mass by a factor of 2. Fig. 6 displays this effect for  $\nu^+ = 0$  DR rate coefficient. The rates decrease by a factor between 10 at 1000 K and 3 at 8000 K, due to lowering of the  $\text{ArD}^+$  ground state, compared to that of  $\text{ArH}^+$ .

### 3.1 Astrophysical consequences

As stated previously,  $\text{ArH}^+$  DR is an important destruction mechanism in interstellar conditions. We have examined two different environments where this molecular ion has been found and have varied the value of the DR rate coefficient over a range of values between  $10^{-9}$  and  $10^{-18}$   $\text{cm}^3 \text{s}^{-1}$  for a sample of 0D steady state chemical models. We solve the coupled  $\frac{d}{dt}[X] = 0$  differential equations where  $[X]$  stands for the abundance of a particular X molecule included in the chemical network for a fixed value of density and temperature and different values of the DR chemical rate coefficient of  $\text{ArH}^+$ ,  $k_{\text{DR}}(\text{ArH}^+)$ . In Fig. 7(a), we display the different solutions of the argonium relative abundance as a function of  $k_{\text{DR}}(\text{ArH}^+)$  for typical diffuse cloud conditions: Proton density  $n_{\text{H}} = 100 \text{ cm}^{-3}$ , temperature  $T = 100$  K,  $\text{H}_2$  cosmic ionization rate  $\zeta = 10^{-16} \text{ s}^{-1}$ , visual extinction  $A_{\text{V}} = 0.001$  and standard interstellar radiation field defined by the scaling parameter  $\chi = 1$ . In Fig. 7(b), we display the different solutions for physical conditions pertaining to the Crab nebula, as discussed in Priestley et al. (2017), *i.e.*  $n_{\text{H}} = 2000 \text{ cm}^{-3}$ ,  $T = 1000$  K,  $\text{H}_2$  cosmic ionization rate

$\zeta = 5 \cdot 10^{-10} \text{ s}^{-1}$ ,  $\chi = 60$ ,  $A_{\text{V}} = 0.1$  and the elemental abundances displayed in Table 1 of Priestley et al. (2017). Each point corresponds to a specific model results and the line connects the different model results. In the standard diffuse cloud conditions, we see that the argonium relative abundance remains constant for values of  $k_{\text{DR}}(\text{ArH}^+)$  smaller than some  $10^{-11} \text{ cm}^3 \text{ s}^{-1}$ , where another destruction mechanism such as photodissociation becomes dominant. It should also be noticed that the scale is linear and the variations are moderate. However, in the extreme conditions of the Crab nebula where the cosmic ionization rate is about 7 orders of magnitude larger, the variation of the relative fractional abundance of argonium is much more spectacular. The limiting value of  $k_{\text{DR}}(\text{ArH}^+) = 10^{-13} \text{ cm}^3 \text{ s}^{-1}$ , below which the relative abundance of argonium remains almost stable and the destruction by photodissociation and reaction with  $\text{H}_2$  take over the dissociative recombination. Our theoretical computations demonstrate that the actual value is significantly below the experimental upper limit  $10^{-9} \text{ cm}^3 \text{ s}^{-1}$  and even below the limiting values stressed out by the models (see Fig. 3(b)). Within these findings, we conclude that DR plays a negligible role in astrophysical media and that photodissociation and reactions with molecular hydrogen become the main destruction processes.

## 4 CONCLUSIONS

In this paper we explored the superexcited states of  $\text{ArH}$  within the R-matrix approach and we computed the cross sections and the corresponding rate coefficients for the dissociative recombination and the vibrational excitation of  $\text{ArH}^+$  by using Multichannel Quantum Defect Theory. The very low values of the dissociative recombination rate coefficients leads to the conclusion that the only significant  $\text{ArH}^+$  destruction mechanisms in the interstellar medium are the collisions with  $\text{H}_2$  molecules and the photodissociation.

## ACKNOWLEDGEMENTS

ER, IFS and VL acknowledge the Programme National "Physique et Chimie du Milieu Interstellaire" (PCMI) of CNRS/INSU with INC/INP co-funded by CEA and CNES. They also thank for generous financial support from La Région Haute-Normandie *via* the GRR Electronique, Energie et Matériaux, from the "Fédération de Recherche Energie, Propulsion, Environnement", and from the LabEx EMC<sup>3</sup> and FEDER *via* the projects PicoLIBS (ANR-10-LABEX-09-01), EMoPlaF and CO<sub>2</sub>-VIRIDIS. IFS and VL thank PHC GALILEE 2018 PROJET (39379SF) and the GdR THEMS. IFS and JZM acknowledge support from the IAEA *via* the Coordinated Research Project "Light Element Atom, Molecule and Radical Behaviour in the Divertor and Edge Plasma Regions". JZM acknowledges support from USPC *via* ENUMPP and Labex SEAM. This work is supported by BATTUTA Project (Building Academic Ties Towards Universities through Training Activities) in the frame of the Erasmus Mundus program, at LOMC UMR-CNRS-6294 of Le Havre University. YM thanks the SRI department, especially Mrs. Martine Currie, for outstanding hospitality.

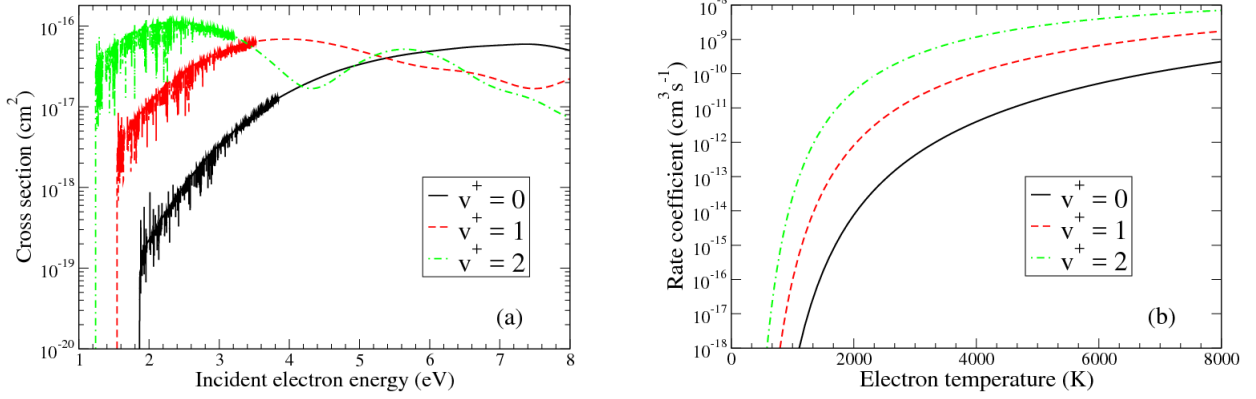


**Figure 3.** Dissociative recombination of ArH<sup>+</sup> on its lowest vibrational levels: (a) global cross sections, coming from the sum over all the available dissociative states; (b) the corresponding Maxwellian-averaged rate coefficients.

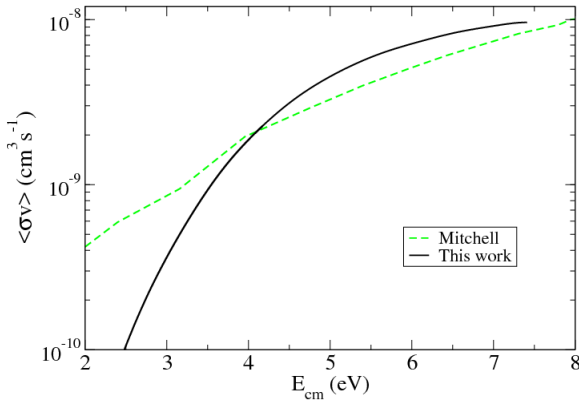


**Figure 4.** Dissociative recombination of vibrationally relaxed ArH<sup>+</sup>. Comparison between the rate coefficient measured in the CRYRING storage ring Mitchell et al. (2005) and the anisotropic rate coefficient obtained by the convolution of our MQDT-computed cross section using the temperatures characterizing the relative velocities of the electrons with respect to the ions in the experiment.

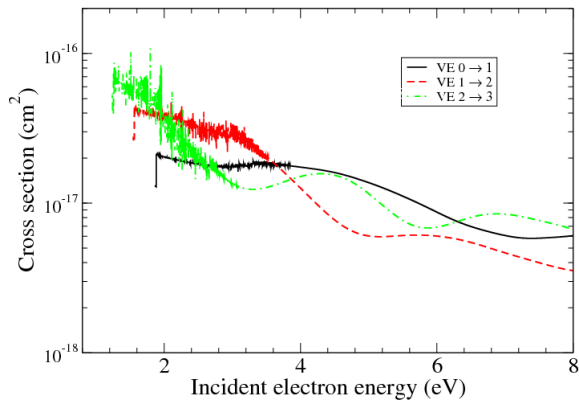


**Figure 5.** Vibrational excitation (VE) of ArH<sup>+</sup> on its lowest vibrational levels: Cross sections for  $\Delta v^+ = 0$  (solid lines). The dissociative recombination (DR) cross section are also shown for comparison (broken line).

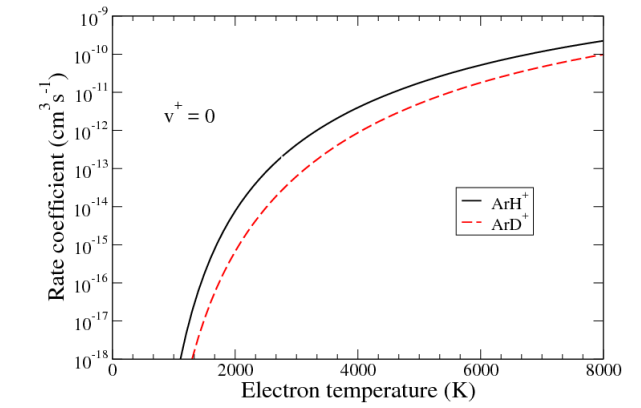


**Figure 6.** Dissociative recombination rate of vibrationally relaxed ArH<sup>+</sup> and ArD<sup>+</sup> as a function of electron temperature: The isotopic effects.

## REFERENCES

- Alekseyev A. B., Liebermann H., Buenker R. J., 2007, *Physical Chemistry Chemical Physics*, 9, 5088
- Barlow M. J., et al., 2013, *Science*, 342, 1343
- Carr J. M., et al., 2012, *The European Physical Journal D*, 66, 58
- Chakrabarti K., et al., 2013, *Phys. Rev. A*, 87, 022702
- Epée Epée M. D., Mezei J. Z., Motapon O., Pop N., Schneider I. F., 2015, *MNRAS*, 455, 276
- Faure A., Gorfinkiel J. D., Morgan L. A., Tennyson J., 2002, *Computer Physics Communications*, 144, 224
- Giusti A., 1980, *Journal of Physics B: Atomic and Molecular Physics*, 13, 3867
- Guberman S. L., Giusti-Suzor A., 1991, *The Journal of Chemical Physics*, 95, 2602
- Hamilton J. R., Faure A., Tennyson J., 2016, *Monthly Notices of the Royal Astronomical Society*, 455, 3281
- Hotop H., Roth T. E., Ruf M.-W., Yencha A. J., 1998, *Theoretical Chemistry Accounts*, 100, 36
- Jungen C., Roche A. L., Arif M., 1997, *Philosophical Transactions of the Royal Society of London A: Mathematical, Physical and Engineering Sciences*, 355, 1481
- Kirrandar A., Child M. S., Stolyarov A. V., 2006, *Phys. Chem. Chem. Phys.*, 8, 247
- Kramida A., Yu. Ralchenko Reader J., and NIST ASD Team 2018, NIST Atomic Spectra Database (ver. 5.5.2), NIST Atomic Spectra Database (ver. 5.5.2), [Online]. Available:

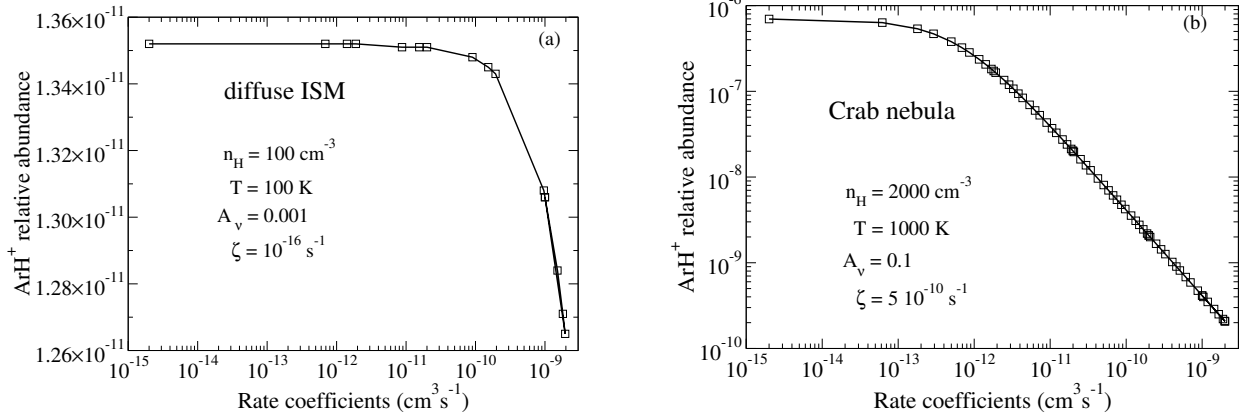


**Figure 7.** Relative abundance of  $\text{ArH}^+$  as a function of the rate coefficients for the case of (a) diffuse ISM (temperature  $T = 100$  K) and (b) Crab nebula (temperature  $T = 1000$  K).

- <https://physics.nist.gov/asd> [2018, January 30]. National Institute of Standards and Technology, Gaithersburg, MD.
- Little D. A., Tennyson J., 2014, *Journal of Physics B: Atomic, Molecular and Optical Physics*, 47, 105204
- Little D. A., Chakrabarti K., Mezei J. Z., Schneider I. F., Tennyson J., 2014, *PHYSICAL REVIEW A*, 90, 052705
- Mitchell J. B. A., et al., 2005, *Journal of Physics B: Atomic, Molecular and Optical Physics*, 38, L175
- Motapon O., et al., 2014, *Phys. Rev. A*, 90, 012706
- Müller H. S. P., et al., 2015, *Astronomy & Astrophysics*, 582, L4
- Neufeld D. A., Wolfire M. G., 2016, *The Astrophysical Journal*, 826, 183
- Priestley F. D., Barlow M. J., Viti S., 2017, *Monthly Notices of the Royal Astronomical Society*, 472, 4444
- Roueff E., Alekseyev A. B., Bourlot J. L., 2014, *Astronomy & Astrophysics*, 566, A30
- Schilke P., et al., 2014, *Astronomy & Astrophysics*, 566, A29
- Stolyarov A. V., Child M. S., 2005, *Phys. Chem. Chem. Phys.*, 7, 2259
- Tennyson J., 1996, *Journal of Physics B: Atomic, Molecular and Optical Physics*, 29, 6185
- Tennyson J., 2010, *Physics Reports*, 491, 29
- Tennyson J., Noble C. J., 1984, *Computer Physics Communications*, 33, 421

## APPENDIX A: SOME EXTRA MATERIAL

The numerical data for  $\text{ArH}^+$  dissociative recombination rate coefficients corresponding to the Fig. 3(b) can be found as supplementary material to this paper.

This paper has been typeset from a  $\text{T}_{\text{E}}\text{X}/\text{L}_{\text{A}}\text{T}_{\text{E}}\text{X}$  file prepared by the author.